MRI Assisted Motion Correction in Dual-Gated 5D Myocardial Perfusion PET Imaging

Jing Tang, *Member, IEEE*, Neal Hall, and Arman Rahmim, *Member, IEEE*

***Abstract*–Involuntary organ movement causes degradation in myocardial perfusion (MP) positron emission tomography (PET) imaging. Respiratory and/or cardiac gating reduces motion while lowering statistics in the reconstructed image frames. The advent of integrated PET/magnetic resonance imaging (MRI) provides opportunities for motion-compensated PET imaging using MRI measured motion. The purpose of this study is to correct respiratory and cardiac motion in dual-gated MP PET imaging, with non-rigid cardiac motion estimated from corresponding cardiac-gated MR images. Using the XCAT phantom, we simulated five-dimensional (5D) dual-gated PET data with and without MP defects and the corresponding 4D cardiac-gated MR images. For each cardiac gate, we performed integrated 4D respiratory motion-corrected image reconstruction to the respiratory-gated data, using the end-expiratory frame as the reference. Then we estimated cardiac motion from the gated MR images using an optical-flow determination algorithm. Using the cardiac motion fields, we warped and summed the respiratory motion-corrected cardiac-gated PET images with the end-diastolic frame as the reference. To evaluate the proposed technique, we performed receiver operating characteristic (ROC) analysis for MP defect detection using a channelized Hotelling observer. The ROC analysis resulted in an area under the curve (AUC) value of .96 ± .02 from images obtained using the proposed respiratory and cardiac motion compensation technique and an AUC value of .85 ± .04 from images reconstructed without motion correction. The proposed MRI assisted motion-corrected image reconstruction technique for dual-gated PET imaging is demonstrated to significantly improve the MP defect detection, which is promising for applications especially in emerging integrated PET/MRI.**

I. Introduction

MYCARDIAL emission computed tomography imaging plays an important role in the diagnostic/prognostic evaluation and follow-up of coronary artery disease [1-3]. To reduce degradation of myocardial perfusion (MP) image quality caused by involuntary organ movement, cardiac and/or respiratory gating has been implemented in clinical or preclinical studies [4]. While gating reduces cardiac and/or respiratory motion blur in the image frames, it also lowers the statistics, i.e., the signal to noise ratio of the reconstructed images. We recently developed a four-dimensional (4D) respiratory motion-corrected MP positron emission tomography (PET) image reconstruction technique and showed that it outperformed conventional imaging qualitatively and quantitatively [5].

With the very recent advent of integrated PET/ magnetic resonance imaging (MRI) [6], a few works (e.g. [7], [8]) have investigated on motion-compensated PET imaging using motion estimated from simultaneously taken MR images. In this study, we propose to correct for cardiac motion following respiratory motion-corrected PET image reconstruction, using non-rigid motion estimated from cardiac-gated MR images. Using simulated dual-gated MP PET data and cardiac-gated MR images, our goal is to evaluate the proposed method for the task of MP defect detection.

II. Materials and Methods

In this study, we simulated dual-gated MP PET imaging data and the corresponding cardiac-gated MR images. For each given cardiac gate, we performed integrated respiratory motion-corrected image reconstruction. Then we estimated cardiac motion vector fields (MVFs) from consecutive gated MR images. The cardiac MVFs were used to warp the respiratory motion-corrected cardiac frames with respect to a reference cardiac gate, followed by summation of the cardiac gates to obtain a high-statistic dual-motion corrected image. To evaluate the proposed technique, we compared the dual-motion corrected images to the average images with no motion correction in the perfusion abnormality detection task.

A. PET Data Simulation

Using the XCAT phantom [9], we simulated two MP 5D imaging datasets, one with normal perfusion and the other with regionally reduced perfusion. The perfusion defect was a transmural defect spanning 40º over the anterior-lateral region and 1.5 cm over the long-axis direction. Its activity was 10% less than the normal activity. The time activity curves of blood pool, myocardium, and other organs were exacted from Rb-82 PET images of 5 patients with normal cardiac function. They were smoothed and averaged to acquire a set of TACs representing the typical Rb-82 biodistribution [10]. Analytical simulations were performed to generate dually gated noise-free PET data with 5 respiratory and 8 cardiac gates. A respiratory cycle lasts 5 sec and each cardiac beating cycle is 1 sec. The noise-free sinograms were scaled corresponding to 2-min cumulated activity after pre-scan delay of ~ 30 sec to avoid high blood pool activity. For both normal and abnormal perfusion cases, 50 Poisson noise realizations were implemented.

Manuscript received November 16, 2012. This work was supported in part by the U.S. National Science Foundation under grant ECCS-1228091 and U.S. National Institutes of Health under grant 1S10RR023623.

Jing Tang is with the Department of Electrical and Computer Engineering, Oakland University, Rochester, MI 48309 USA (e-mail: jtang@oakland.edu).

Neal Hall is with the Department of Radiology, St. Joseph Mercy Oakland Hospital, Pontiac, MI 48340 USA.

Arman Rahmim is with the Department of Radiology, The Johns Hopkins University, Baltimore, MD 21287 USA.

B. MR Image Simulation

The MR image simulation was performed using the open source simulator SIMRI [11], which we modified to take the T1, T2, and proton density maps created using the XCAT phantom with known tissue values. SIMRI takes into account the main static field value and enables realistic simulations of the chemical shift artifact including off-resonance phenomena. To simulate a protocol used in the clinical PET/MR scanner, we specified the sequence to be 3D T1-weighted (turbo spin echo, echo time/repetition time = 2.3 ms/4 ms) with low flip angle of 2º [12]. We simulated the 8 cardiac gates at the end-expiratory gate, as it was used as the reference gate for respiratory motion correction.

C. Respiratory Motion Corrected Image Reconstruction

Before applying 4D EM reconstruction to the respiratory-gated data, we first reconstructed images from data rebinned into respiratory-only gates followed by respiratory motion estimation. This is more robust compared to estimating motion from images that are additionally cardiac-gated. The respiratory motion was assumed to be rigid and the translation vectors were first estimated using least-squares difference minimization via the BFGS Quasi-Newton method with a cubic line search procedure [13].

For a given cardiac gate, we applied 4D EM reconstruction to the respiratory-gated data within the specific cardiac phase. Given an image estimate vector $\boldsymbol{\lambda}^k$, respiratory-gated data $\mathbf{y}_n$ (n = 1, …, *N*) within the given cardiac gate, the system matrix $\mathbf{P}$, and the respiratory motion operator $\mathbf{M}_{1\to n}$ that maps the reference respiratory gate 1 to any given respiratory gate n, the 4D motion-corrected reconstruction algorithm can be written as:

$$\boldsymbol{\lambda}^{k+1} = \frac{\boldsymbol{\lambda}^k}{\sum_{n=1}^{N} \mathbf{M}_{1\to n}^T \mathbf{P}^T \mathbf{1}} \sum_{n=1}^{N} \mathbf{M}_{1\to n}^T \mathbf{P}^T \frac{\mathbf{y}_n}{\mathbf{P}\mathbf{M}_{1\to n}\boldsymbol{\lambda}^k} \quad , \qquad (1)$$

where multiplication and division of vectors are performed element-wise, *T* indicates the transpose, and $\mathbf{1}$ is a column vector with all elements equal to 1.

D. Cardiac Motion Estimation and Correction

We estimated the cardiac motion from the simulated cardiac-gated MR images before using the cardiac MVFs to warp the reconstructed images acquired in the above subsection. The cardiac motion estimation was treated as a constrained minimization problem [14]. The estimation problem is solved by finding the MVF $\mathbf{m}$ that minimizes the cost function $E_I(\mathbf{m}) + \alpha E_S(\mathbf{m})$, where $E_I(\mathbf{m})$ is the image-matching error term and $E_S(\mathbf{m})$ is a regularization term with α as the weight. The image-matching error is defined as the intensity difference between the normalized first frame and the warped correspondence of the normalized second frame with a given MVF $E_I(\mathbf{m}) \triangleq \sum_{\mathbf{r}} [f_1(\mathbf{r}) - f_2(\mathbf{r} + \mathbf{m}(\mathbf{r}))]^2$, (2)

where $\mathbf{r}$ is the 3D spatial coordinate of a voxel, f_1 and f_2 are the intensity images from which an MVF is to be estimated, $\mathbf{m}$ is the 3D MVF that supposedly warps f_2 to f_1. The strain energy function for a linear isotropic elastic material is chosen to serve as the regularizing constraint [15]. The MVF is estimated using an iterative method that updates the current estimate by minimizing the quadratic approximation of the cost function.

Using the cardiac MVFs estimated from the simulated MR images, we corrected the cardiac motion of the respiratory motion-corrected images described in II.C. The end-diastolic frame (the 1st cardiac gate) was used as the reference gate and the motion corrected summation starts from the last gate (the 8th gate). To be more specific, the 8th gate was warped using the MVF estimated from the 7th and 8th frames and added to the 7th image. Then the motion-corrected summation of the 8th and 7th images was warped using the MVF from the 6th and the 7th images and added to the 6th image, and so on.

E. Perfusion Defect Detection Analysis

To evaluate the reconstructed images using the proposed techniques described above, we performed receiver operating characteristic (ROC) analysis for the MP defect detection task. We used a channelized Hotelling observer (CHO) with four octave-wide rotationally symmetric frequency channels to generate ratings for the defect-absent and defect-present images [16]. The resulting ratings acquired from the CHO were used to estimate ROC curves with the LABROC4 program [17]. This program estimates the parameters of the ROC curve, the area-under-curve (AUC) value and the standard deviations of these parameters. We compared the ROC estimates from images with and without the proposed respiratory and cardiac motion correction using the CLABROC program [18].

III. Results

The simulated cardiac-gated MR images from which cardiac MVFs were estimated are shown in Fig. 1, one transaxial slice from each of the 8 cardiac gates. To demonstrate the effect of respiratory motion correction, we present the reconstructed PET images from the data of end-diastolic gate (the 1st cardiac gate) in Fig. 2 and Fig. 3. The images were rotated and cropped for the CHO application, with the centroid of the defect region at the center. Fig. 2 shows four (out of the 50) noise realizations of images reconstructed with no respiratory motion correction, without and with the perfusion defect. Fig. 3 shows the images reconstructed with the integrated motion-correction algorithm described in II. C. Comparing Fig. 2 and Fig. 3, we are able to see the difference resulted from respiratory motion correction. The images in Fig. 2 have the blur in the vertical direction, which is caused by averaging the respiratory gates. The blur is significantly reduced as seen in images of Fig. 3.

Fig. 4 and Fig. 5 show images reconstructed with the data of all the cardiac and respiratory gates. The images in Fig. 4 were acquired by summing the cardiac gates that were reconstructed without respiratory motion correction. The images in Fig. 5 were obtained with motion correction among respiratory motion-corrected cardiac gates, as described in II. D. Besides the respiratory blur reduction, we can also see that the blood pool in images of Fig. 5 appears larger than that in images of

Fig. 4. This demonstrates the effect of cardiac motion correction with the end-diastolic gate as the reference frame.

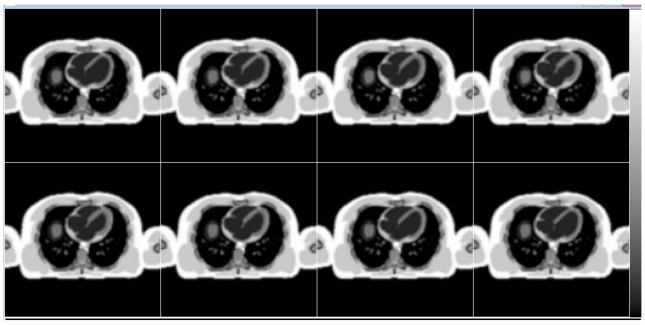

Fig. 1. Transaxial slices of simulated cardiac-gated MR images (starting from the end-diastolic frame), from which cardiac MVFs were estimated for PET image motion correction.

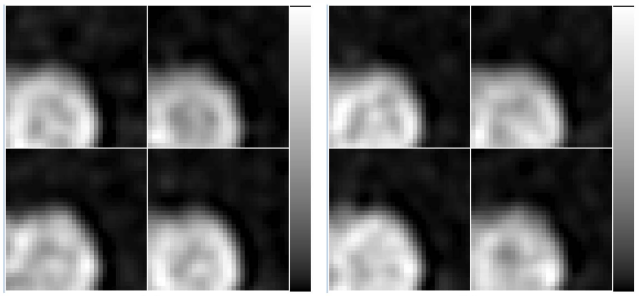

(a) (b)

Fig. 2. PET images of cardiac gate 1 with no respiratory motion correction, short-axis view processed with the centroid of defect region at the center, 4 noise realizations (a) without and (b) with perfusion defect.

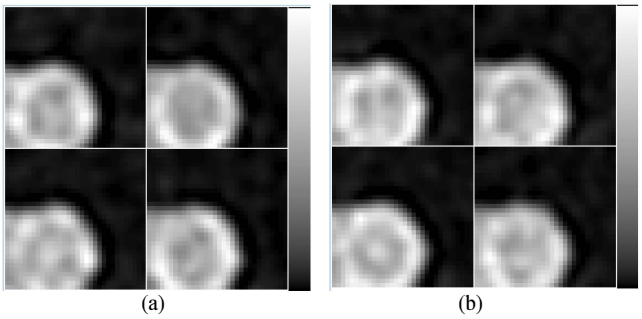

(a) (b)

Fig. 3. PET images of cardiac gate 1 with respiratory motion correction, short-axis view processed with the centroid of defect region at the center, 4 noise realizations (a) without and (b) with perfusion defect.

Fig. 6 (a) shows the results from ROC analysis for images of cardiac gate 1 without and with respiratory motion correction, corresponding to images displayed in Fig. 2 and Fig. 3. The AUC values are .56 ± .06 and .68 ± .05 for cases without and with respiratory motion correction, respectively. The CLABROC test indicated that the difference between the two ROC curves was statistically significant with the two-tailed p-value as 0.04. Fig. 6 (b) shows the ROC curves for images reconstructed from all cardiac and respiratory frame data, one with no motion correction corresponding to images as shown in Fig. 4, the other with respiratory and cardiac motion correction for images as shown in Fig. 5. The AUC values are .85 ± .04 and .96 ± .02, respectively. The CLABROC test on these two ROC curves indicated that the proposed respiratory and cardiac motion correction technique significantly improves MP defect detection (two-tailed p-value less than 0.01).

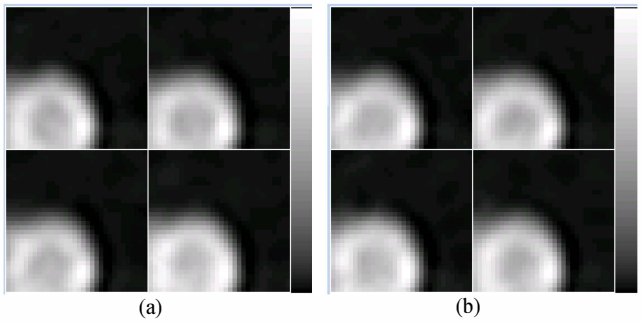

(a) (b)

Fig. 4. PET images with no respiratory or cardiac motion correction, short-axis view processed with the centroid of defect region at the center, 4 noise realizations (a) without and (b) with perfusion defect.

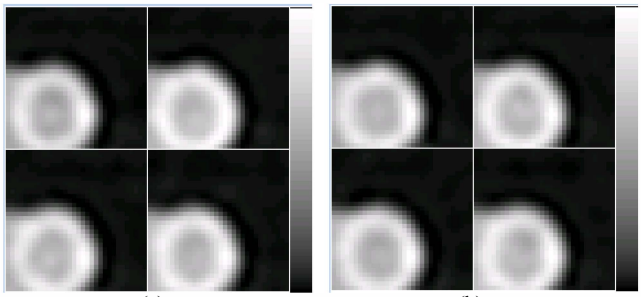

(a) (b)

Fig. 5. PET images with respiratory and cardiac motion correction, short-axis view processed with the centroid of defect region at the center, 4 noise realizations (a) without and (b) with perfusion defect.

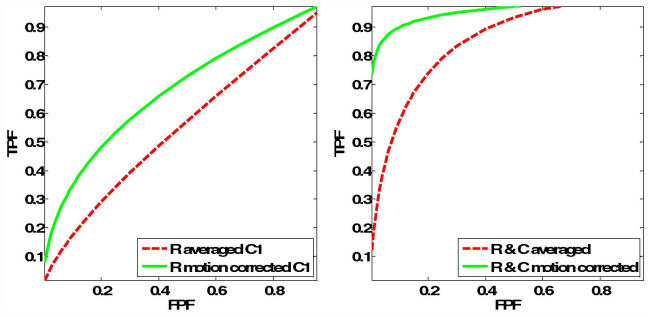

(a) (b)

Fig. 6. ROC plots, true positive fraction (TPF) vs. false positive fraction (FPF) for the task of MP defect detection. (a) for cardiac gate 1, with and without respiratory (R) motion correction; (b) for all frame data, with R and cardiac (C) motion correction and without motion correction.

IV. Conclusions

We developed a 5D motion-corrected PET image reconstruction algorithm for dual-gated MP imaging, using cardiac motion estimated from corresponding gated MR images. Using simulated dual-gated PET data and cardiac-gated MR images, we demonstrated that the proposed technique significantly improved the PET imaging performance for the task of MP defect detection. The approach will have promising applications especially in the emerging integrated PET/MRI.

ACKNOWLEDGMENT

We thank Dr. Nikolaos A. Karakatsanis for computational support.

REFERENCES

[1] R. Hachamovitch and D. S. Berman, "The use of nuclear cardiology in clinical decision making," *Semin Nucl Med,* vol. 35, pp. 62-72, Jan 2005.

[2] M. I. Travin and S. R. Bergmann, "Assessment of myocardial viability," *Semin Nucl Med,* vol. 35, pp. 2-16, Jan 2005.

[3] J. Machac, "Cardiac positron emission tomography imaging," *Semin Nucl Med,* vol. 35, pp. 17-36, Jan 2005.

[4] A. Rahmim, O. G. Rousset, and H. Zaidi, "Strategies for motion tracking and correction in PET.," *PET Clinics,* vol. 2, pp. *251-266*, 2007.

[5] A. Rahmim, J. Tang, M. R. Ay, and F. Bengel, "4D respiratory motion-corrected Rb-82 myocardial perfusion PET image reconstruction," *IEEE Nucl Sci Symp Conf Record ,* pp. 3312-3316, 2010.

[6] B. J. Pichler, A. Kolb, T. Nagele, and H. P. Schlemmer, "PET/MRI: paving the way for the next generation of clinical multimodality imaging applications," *J Nucl Med,* vol. 51, pp. 333-6, Mar 2010.

[7] B. Guerin, S. Cho, S. Y. Chun, X. Zhu, N. M. Alpert, G. El Fakhri, T. Reese, and C. Catana, "Nonrigid PET motion compensation in the lower abdomen using simultaneous tagged-MRI and PET imaging," *Med Phys,* vol. 38, pp. 3025-3038, Jun 2011.

[8] C. Catana, T. Benner, A. van der Kouwe, L. Byars, M. Hamm, D. B. Chonde, C. J. Michel, G. El Fakhri, M. Schmand, and A. G. Sorensen, "MRI-assisted PET motion correction for neurologic studies in an integrated MR-PET scanner," *J Nucl Med,* vol. 52, pp. 154-61, Jan 2011.

[9] W. P. Segars, D. S. Lalush, and B. M. W. Tsui, "A realistic spline-based dynamic heart phantom," *IEEE Trans Nucl Sci,* vol. 46, pp. 503-506, Jun 1999.

[10] J. Tang, A. Rahmim, R. Lautamaki, M. A. Lodge, F. M. Bengel, and B. M. Tsui, "Optimization of Rb-82 PET acquisition and reconstruction protocols for myocardial perfusion defect detection " *Phys Med Biol,* vol. 54, pp. 3161-71, 2009.

[11] H. Benoit-Cattin, G. Collewet, B. Belaroussi, H. Saint-Jalmes, and C. Odet, "The SIMRI project: a versatile and interactive MRI simulator," *J Magn Reson,* vol. 173, pp. 97-115, Mar 2005.

[12] V. Schulz, I. Torres-Espallardo, S. Renisch, Z. Hu, N. Ojha, P. Bornert, M. Perkuhn, T. Niendorf, W. M. Schafer, H. Brockmann, T. Krohn, A. Buhl, R. W. Gunther, F. M. Mottaghy, and G. A. Krombach, "Automatic, three-segment, MR-based attenuation correction for whole-body PET/MR data," *Eur J Nucl Med Mol Imaging,* vol. 38, pp. 138-152, Jan 2011.

[13] D. F. Shanno, "Conditioning of quasi-Newton methods for function minimization," *Math of Comput,* vol. 24, pp. 647-656, 1970.

[14] J. Tang, W. P. Segars, T. S. Lee, X. He, A. Rahmim, and B. M. Tsui, "Quantitative study of cardiac motion estimation and abnormality classification in emission computed tomography," *Med Eng Phys,* vol. 33, pp. 563-72, Jun 2011.

[15] A. E. H. Love, *A treatise on the mathematical theory of elasticity* Cambridge: Cambridge University Press, 1944.

[16] S. D. Wollenweber, B. M. W. Tsui, E. C. Frey, D. S. Lalush, and K. J. LaCroix, "Comparison of human and channelized Hotelling observers in myocardial defect detection in SPECT," *J Nucl Med,* vol. 39, p. 771A, 1998.

[17] C. E. Metz, J. H. Shen, and B. A. Herman, "New methods for estimating a binormal ROC curve from continuously distributed test results," in *Ann. Meeting of the American Statistical Association*, Anaheim, CA, 1990.

[18] C. E. Metz, B. A. Herman, and C. A. Roe, "Statistical comparison of two ROC-curve estimates obtained from partially-paired datasets," *Med Decis Making,* vol. 18, pp. 110-121, Jan-Mar 1998.